A global model for the combustion of gas mixtures released from forest fuels

Determination of a global combustion mechanism for flaming in forest fire modelling

VIRGINIE TIHAY[a], ALBERT SIMEONI[a], PAUL-ANTOINE SANTONI[a], JEAN-PIERRE GARO[b] AND JEAN-PIERRE VANTELON[b]

[a] SPE– UMR 6134 CNRS, University of Corsica, Campus Grossetti, BP 52, 20250 Corte, France

[b] LCD – UPR 9028 CNRS, ENSMA, University of Poitiers, 1 avenue Clément Ader, Téléport 2 – BP 40109, 86961 Futuroscope Chasseneuil Cedex, France

Corresponding author:

Virginie Tihay

SPE – UMR 6134 CNRS, University of Corsica, Campus Grossetti, B.P. 52, 20250 Corte, France,

Phone: +33 495 450 121, Fax: +33 495 450 162,

E-mail address: *tihay@univ-corse.fr*

Colloquium topic: Fire research

Alternate Colloquium topic: Laminar flames

Total Paper length determined by using method 1: 5565 words

Main text: 1508+365+18+43+8+1244=3184

Equations: 137+23+53+23+30=266

References: 280

Tables and captions: 219

Table 1: 106 Table 2: 113

Figures and captions: 1617

Fig. 1: 262 Fig. 2: 140 Fig. 3: 125 Fig. 4: 139 Fig. 5: 145

Fig. 6: 402 Fig. 7: 403

Abstract – The aim of this study is the improvement of the combustion modelling in forest fires. To proceed, the degradation gases released by Mediterranean forest fuels have been determined. They mainly consist of CO_2, CO, CH_4 and H_2O. Then, an experimental device was built to produce laminar, axisymmetric, time-varying and non-premixed flames from these vegetative fuels. The collected data (temperature, flame radius and mass flow rate) have been used to implement and validate the combustion modelling. Using numerical methods, the transient equations for the conservation of mass, momentum, energy and chemical species have been solved for the flame as well as the radiative transfer equation. Three combustion mechanisms have been tested: a skeletal mechanism, a global mechanism currently applied in forest fire incorporating only carbon monoxide and an original global mechanism with three reactions including methane and carbon monoxide. The comparison between the experimental and predicted results shows that the model containing only carbon monoxide underestimates significantly the temperature in the fire plume. On the contrary, the results obtained with the skeletal and the three-step mechanism including both methane and carbon are in good agreement with the experimental data. This study underlines also the necessity to include methane in the gas oxidation model to improve the predictions in wildland fire modelling.

Keywords: forest fire; gas combustion modelling

1 Introduction

Wildland fires are an annually occurring threat to people and property in many nations of the world. Over the last sixty years, a significant amount of interest in numerical modelling of wildland fire spread has been generated within the scientific community. Three types of modelling approaches have emerged. The first one includes statistical models [1]. The second one incorporates empirical models [2]. Based on a detailed description of the heat transfer mechanisms, which govern the fire propagation, the physical models [3-5] are the third set of models. However, even in the most sophisticated approaches, the degradation gases and the combustion in gas phase are not treated in detail. The combustible part of the devolatilization products is generally considered to be solely carbon monoxide burning in air [6], whatever vegetation species.

The aim of this study is to provide a simple reliable model for the oxidation of the degradation gases, which could be included in a model of wildand fire. To proceed, experiments are carried out first to collect data for the implementation and to validate a numerical model. The gases released during the degradation of three Mediterranean forest fuels are analysed by using a tube furnace connected either to a gas chromatograph or to a hygrometer. An experimental device is built in order to generate unsteady, axisymmetric, non-premixed laminar flames from the forest fuels. The mass flow rate, the flame radius and the distribution of temperature are recorded. Next, a primitive variable formulation is used to solve the transient conservation equations of mass, momentum, energy, species as well as radiation. Three combustion mechanisms are tested. The first one is the skeletal mechanism given by Peters *et al* [7]. It is used to determine the composition of the gases released in the numerical domain and to serve as reference model. The second one is a global reaction mechanism based on Grishin's hypothesis [6]. Finally, the last one is an original combustion mechanism including three global reactions and taking into account carbon monoxide and methane. The numerical results obtained with the three mechanisms are compared to the experimental data and discussed in order to propose a simple combustion model.

2 Experimental Devices

All experiments were conducted with three fuels: *Pinus halepensis, Pinus laricio* and *Erica arborea*. Before experiments, the plants were oven-dried at 60°C during 24 hours and then they were crushed and sieved to a particle size of 0.6-0.8 mm. It allows first decreasing the influence of the geometry of forest fuels on their combustion and then producing laminar flames what permits to study the combustion kinetics hidden in the turbulent flames.

2.1 Analysis of degradation gases

The composition of the degradation gases was determined thanks to a tube furnace apparatus used as pyrolyser. Thermogravimetric analysis showed that the samples mainly degrade between 280 and 425°C [8]. Thus, we only analysed the gas mixture released during this range of temperature under nitrogen. The combustion chamber was filled with 4 g of sample. Gases were collected into a gas sampler. Then, the gas sampler was directly attached either to the gas chromatograph (Flame Ionization Detector and Thermal Conductivity Detector) or to the hygrometer (EdgeTech Model 2001 Series DewPrime) measuring the dew point with a resolution of 0.1°C. The mass loss of the sample between 280 and 425°C was measured for each run. At least three repetitions were carried out for each species.

2.2 Burning experiments

The burning experiments were performed in order to collect data to implement and to validate the numerical model. The fuel bed was in the shape of a cylinder with a diameter of 3.5 cm, a depth of 0.5 mm and a mass of 1.5 g. It was positioned on a load cell in order to measure the fuel mass loss as

a function of time. To insure a fast and homogeneous ignition, a small amount of ethanol (0.7 mL) was spread uniformly on the fuel bed and was ignited with a flame torch. An array of 11 thermocouples was positioned above the fuel bed along the flame axis. The first thermocouple was placed 1 cm above the top of the support and the others were located 1 cm from each other. A second array of 7 thermocouples was situated horizontally. The spacing between the thermocouples was equal to 5 mm. All the thermocouples used were mineral-insulated integrally metal-sheathed pre-welded type K (chromel-alumel) pairs of wire with an exposed junction. At the exposed junctions the wires were 50 μm in diameter. The uncertainty in temperature and mass measurements was respectively 0.5°C and 2.5 %. Two visual cameras allowed observing the regression of the flame height and of the flame basis. The ambient temperature was close to 21°C and the relative humidity was around 50 %. At least five repetitions were made to collect reliable data.

3 Experimental Results

3.1 Degradation gases

Table 1 shows the main degradation gases analysed for the three fuels. Degradation gases mainly consist of CO_2, CO, CH_4, H_2O, and lower amounts of H_2 and C_2, C_3 and C_4 hydrocarbons. However, the mass fractions change among the forest fuels. The highest quantity of combustible gases is obtained by *Pinus laricio* (31 %), followed by *Pinus halepensis* (26.7 %) and *Erica arborea* (23.5 %). The two pines have a close mass fraction of water whereas *Erica arborea*'s one is twice lower. Based on these analyses, the heating value per mass of air for each gas composition is 3.23, 3.18 and 3.27 $MJ.kg_{air}^{-1}$ respectively for *Pinus halepensis*, *Pinus laricio* and *Erica arborea*. Theses values are close for the three fuels.

3.2 Flame characteristics

This part exhibits a quick description of the flame characteristics. We present the quantities used either for the input in the simulation or for the validation of the numerical results.

3.2.1 Flame behaviour

For the three forest fuels, three different stages are observed during the fuel burning: the ignition, the flame regression and the extinction. The first stage lasts around 60 s and corresponds to a flickering flame due to the presence of ethanol to ignite the sample. During the second stage, the fuel is only composed of the degradation gases as the ethanol is completely burned. The flame becomes laminar and decreases slowly. The last stage concerns the extinction of the flame. The remaining solid phase is essentially composed of carbon at the sample surface with a certain amount of unburned fuel near the support. Contrary to the other samples, the remaining solid phase of *Erica arborea* is covered by tar. The combustion time lasts around 180 s.

3.2.2 Mass loss

The mean mass loss is approximated by 4th order polynomials (Fig. 1.a). During the ignition stage, a steep decrease mainly due to the burning of ethanol is observed. Next, the mass loss slows down during the regression stage. Figure 1.b. presents the mean mass loss rate for the three fuels during the regression and the extinction stage. The stage changing is characterized by an inflexion point on the mass flow rate curves (around 120 s). During the regression stage, the highest mass flow rate is obtained by *Pinus halepensis* followed by *Erica arborea* and *Pinus laricio*. These data are used in the simulation to set the mass flow inlet of degradation gases. After 120 s, the mass flow rate of the two pines is close whereas *Erica arborea*'s one decreases quickly because of the tar production, which settles on the sample surface reducing the mass loss.

3.2.3 Flame radius

Figure 2 presents the time evolution of the mean radiuses of the flame after 60 s approximated with quadratic polynomials. As the flame decreases during the regression and the extinction stage, the flame radius diminishes slowly from around 1.6 to 0.4 cm. The flame base of *Pinus laricio* regresses faster than *Pinus halepensis* and *Erica arborea* ones. The approximated polynomials are used in the simulation for setting the radius of the mass flow inlet zone.

3.2.4 Vertical Temperature

The time evolution of the temperature along the flame axis at 1, 2, 3, 4, 5, 7 and 11 cm is only presented for *Erica arborea* (Fig 3) as a same trend is observed for the whole species. During the first 60 s, the curves fluctuate due to the ignition with ethanol. Then, they become smooth during the regression stage. The maximum of the curves corresponds to the crossing of the thermocouples by the reaction zone. For the whole species, it reaches about 1000°C as their heating values per mass of air are similar. As the flame height decreases, only the thermocouples below 3 cm remain in the flame zone. Some fluctuations appear on the curves above 5 cm as these thermocouples record the temperature in the thermal plume, which becomes progressively turbulent. The vertical temperature is used to validate the numerical results.

4 Combustion Modelling and Discussion

4.1 Numerical model

4.1.1 Mathematical formulation

As we focus on the study of the combustion in the gas phase, the fuel bed is represented as a burner. The model solves the two-dimensional, axisymmetric, time-dependant, laminar, reactive-flow Navier-Stokes equations coupled with radiation and transport:

$$\frac{\partial \rho}{\partial t} + \vec{\nabla}\rho\vec{V} = 0 \qquad (1)$$

$$\frac{\partial \rho Y_i}{\partial t} + \rho\vec{V}.\vec{\nabla}Y_i = \vec{\nabla}\left(\rho D_{ij}\vec{\nabla}Y_i\right) + \dot{\omega}_i \qquad (2)$$

$$\frac{\partial \rho \vec{V}}{\partial t} + \rho\vec{V}\vec{\nabla}.\vec{V} = \vec{\nabla}p + \rho\vec{g} + \vec{\nabla}.\bar{\bar{\tau}} \qquad (3)$$

$$\frac{\partial \rho e}{\partial t} + \rho\vec{V}.\vec{\nabla}e = \vec{\nabla}\left(\lambda\vec{\nabla}T\right) + \vec{\nabla}.\vec{R} \qquad (4)$$

$$+\vec{\nabla}\left(\rho\sum_{i=1}^{N} h_i D_{ij}\vec{\nabla}Y_i\right) - \vec{\nabla}.\left(p\,\vec{V}\right) + \vec{\nabla}.\left(\bar{\bar{\tau}}.\vec{V}\right) + \dot{Q}$$

$$\frac{dI\left(\vec{r},\vec{s}\right)}{ds} + a\,I\left(\vec{r},\vec{s}\right) = a\frac{\sigma T^4}{\pi} \qquad (5)$$

where $\dot{\omega}$ is the mass rate of production, $\vec{R}$ is the radiant heat flux, $\dot{Q}$ is the volumetric heat source, I is the radiant intensity, $\vec{r}$ is the direction vector, $\vec{s}$ is the unit vector along the radiant intensity path and a is the absorptivity. The subscripts i and j represent the gas species. The properties (viscosity, density, thermal conductivity and diffusivity…) of the gas species and of the gas mixture

as well as the numerical methods have been determined after a analysis of parameterization and of sensitivity. We have selected the most efficient configuration in term of computational cost and accuracy. The Radiative Transfer Equation (RTE, Eq. 5) is solved using a discrete ordinates method [9] following 144 directions in space. The gas is approximated by a mixture of grey gases containing CO_2 and H_2O. For each gas species, the viscosity and the thermal conductivity are computed using the kinetic theory [10] whereas the specific heat capacity is a function of temperature. As several gases are taken into account, different laws are used for the gas mixture properties. The incompressible ideal-gas law is used to calculate density variations. An ideal gas mixing law specifies the viscosity and the thermal conductivity. A mixing law defines the specific heat capacity and the diffusion coefficients are computed with the kinetic theory. The set of conservation equations in the gas phase is solved numerically by a finite-volume method. Diffusion terms are approximated using a second-order central difference scheme. Convective terms are discretized using a first-order upwind scheme. The pressure-velocity coupling is handled by using the SIMPLE algorithm [11]. The resulting systems of linear algebraic equations are then solved iteratively by using the Algebraic Multigrid algorithm [12].

4.1.2 Chemical mechanisms

To simplify the problem, we only conserve six chemical species (CO_2, CO, CH_4, H_2O and N_2) from the gas analysis (paragraph 3.1). Three combustion mechanisms are tested: a skeletal and two global mechanisms. The skeletal mechanism (SM) is given by Peters *et al* [7]. It was elaborated for methane combustion and consists of 23 reactions and 14 gaseous species. The first global mechanism GM1 only considers carbon monoxide following Grishin's hypothesis. The CO oxidation produces CO_2 and the reverse reaction is taken into account:

$$CO + 0.5O_2 \Leftrightarrow CO_2 \qquad (6)$$

The rates of production of the chemical species are written with Arrhenius's laws and are given by [13]:

$$\dot{\omega}_{CO} = 2.239\,10^{12}[CO][H_2O]^{0.5}[O_2]^{0.25}\exp\left[-\frac{1.3\,10^{8}}{R.T}\right] \quad (7)$$

$$\dot{\omega}_{CO_2} = 5\,10^{8}[CO_2]\exp\left[-\frac{1.3\,10^{8}}{R.T}\right] \quad (8)$$

Mechanism MG2 has been developed for this study and takes into account two fuels: carbon monoxide and methane. The chemical reactions for carbon monoxide are identical to the previous case (Eq. 6 to 8). The methane combustion is incomplete and products carbon monoxide:

$$CH_4 + 1.5O_2 \Rightarrow CO + 2H_2O \quad (10)$$

The rate of production is given by [13]:

$$\dot{\omega}_{CH_4} = 5.012\,10^{11}[CH_4]^{0.7}[O_2]^{0.8}\exp\left[-\frac{2\,10^{8}}{R.T}\right] \quad (11)$$

For all of the mechanisms, the units for the rates of production are kmoles, cubic meters, seconds and Kelvins. The activation energy for carbon monoxide has been developed in [13] for turbulent

combustion and is not adapted for the laminar flow. Thus, it has been decreased until the combustion sustains.

4.1.3 Computational domain and boundary conditions

As the flames are almost conical, an axisymmetric condition is used to decrease the computational time. A rectangle represents the burner. Several tests have been performed concerning the size of the computational domain and of the meshes to ensure that the width of the domain does influenced the flame behaviour and that numerical results are grid-independent. All the computations have been carried out using a Cartesian non-uniform grid covering a space domain of 3.5 cm × 15 cm. The grid contains 66 600 cells with a mesh size of 0.2 mm from z = 0 to 6 cm and from r = 0 to 6 cm along the vertical and radial direction respectively. In the remaining part of the grid, a dilatation ratio of 1.03 is applied along the height. The initial conditions: mass flow rate, burner radius and gas composition are directly deduced from the experimental data. A stationary solution of the flow field is first computed without reaction. Then, the ignition is carried out by applying a temperature of 1200 K near the burner.

4.2 Gas composition released by the burner

The determination of the CO_2, CO, CH_4 and H_2O mass fractions released by the burner is realised with the skeletal mechanism (SM) which takes into account the largest number of species and equations. To proceed, we test two compositions based on the experimental results of *Pinus laricio* at 60 s (beginning of the regression stage). For both mixtures, the mass fractions of CO and H_2O correspond to the values in Table 1. In composition 1, the mass fraction of CH_4 is equal to the value in Table 1. In composition 2, the mass fraction of CH_4 takes into account the heat release of C_2 hydrocarbons (Y_{CH4}=0.062). Finally, the mass fraction of CO_2 is taken to set the sum of all mass fractions equal to 1. Figure 4 presents a comparison between the numerical and the experimental

temperatures along the flame axis (the vertical slashes represent the range of the experimental temperatures). When the composition takes into account C_2 hydrocarbons, the maximum temperature increases of 66°C and its position is shifted 0.72 cm. The results computed with the composition 1 are in very good agreement with the experimental data in the flame area whereas the composition 2 overestimates the values and does not give an account of the combustion kinetics in this zone. In the thermal plume, the both mixture overestimate the temperature. This is due to the laminar modelling that cannot represent the turbulent mixing along the plume. Thus, to match the experiments, the mass fractions of CO, CH_4 and H_2O must be equal to the values obtained during the gas analysis. The other gaseous species have to be neglected and be considered as CO_2. This result is likely a consequence of the modelling which does not take into account the mechanisms of soot production/oxidation. In the following, the skeletal mechanism with composition 1 is defined as reference mechanism.

4.3 Determination of a global mechanism

To compare the two global mechanisms (MG1 and MG2), we use two different gas mixtures derived from the experimental data of *Pinus laricio* at 60 s. For mechanisms SM and MG2, the mass fractions are equal to Y_{CO}=0.140, Y_{CH4}=0.040, Y_{H2O}=0.074 and Y_{CO2}=0.746 (composition 1). For mechanism MG1, the gas mixture is based on Grishin's hypothesis [6], which is currently employed in the multiphase formulation used for the forest fire modelling [5, 14]. In this approach, the combustible part of pyrolysis gases consists only of carbon monoxide. The initial mass fraction of CO is equal to the sum of the initial mass fractions of CO and CH_4 (Y_{CO}=0.180). Figure 5 shows the experimental temperatures and the prediction along the flame axis obtained with the skeletal and the two global mechanisms. Mechanism MG1 underestimates significantly the temperatures and modifies the position of the maximum, which appears 1.4 cm lower. The energy released is too low to describe accurately the temperature in the fire flume and the combustion kinetics is not good represented in the flame. On the contrary, mechanism MG2 products temperatures very close to the

ones of skeletal mechanism. In the zone of maximum reactivity, the temperature is however slightly lower (about 72°C) and but is closer to the experimental one. The incorporation of methane allows also improving the predictions of temperature and combustion kinetics in the fire plume. In view of these results, mechanism MG2 including methane seems better adapted to simulate the laminar flame than mechanism MG1 based on Grishin's hypothesis [6]. This observation highlights the necessity of including methane in combustion modelling in the forest fire models to improve the flame prediction.

4.4 Comparison with Experiment

We have tested mechanism MG2 for the three forest fuels at 80 s. This time is chosen in order to validate the mechanism at different moment of the regression stage. A summary of the initial conditions is presented in Table 2 for the three fuels. Figures 6.a-c present the experimental and predicted temperatures along the flame axis. For the three species, the computed temperatures are in general in a good agreement with the experimental data. The discrepancies between the predicted and the mean experimental temperatures are indeed less than 100°C in the flame zone and the numerical results are still in the range of the experimental data. In the thermal plume, the predictions give a good order of magnitude of temperature even if they tend to overestimate it because of the laminar flow modelling. The experimental and computed temperatures at 1 cm high are presented by the Figure 7 for the three species. The temperature curves are characteristic of diffusion flames and are close to the experimental data for the whole species. The numerical predictions allow also representing the experimental flame shape. According to these results, the global combustion kinetics proposed by this mechanism tallies with the experimental one. In the thermal plume, the simulations provide a good estimation of the temperature decrease. Thus, whatever the forest fuel, the mechanism MG2 supplies numerical results close to the experimental values.

5 Conclusion

In this paper, the composition of degradation gases released by three different Mediterranean species has been determined. Next, mass flow rate, flame radius and temperature distribution have been measured in the unsteady, axisymmetric, non-premixed laminar flames from these fuels. All these data have been used to implement and validate a combustion modelling which takes into account the main degradation gases of the forest fuels.

Numerical predictions have been obtained by solving the transient equations for the conservation of mass, momentum, energy and chemical species as well as the radiative transfer equation. Three different combustion mechanisms have been investigated. Comparison of the experimental results with the model reveals that the mechanism considering only carbon monoxide does not allow reproducing correctly the experimental results for laminar flow. On the contrary, the mechanism with methane produces numerical temperatures close to experimental data. This simple and reliable combustion mechanism includes only three global reactions and provides encouraging results in laminar flows. However, to improve further this gas oxidation model, other studies are necessary to test this model for turbulent condition, for static and spreading flames.

6 References

[1] A.G. McArthur, Weather and grassland fire behaviour, Leafter n°100, Australian Forest and Timber Bureau, 1966.

[2] R.C. Rothermel, A mathematical model for predicting fire spread in wildland fuels, INT-115, USDA Forest Service, 1972.

[3] F.A. Albini, Combust. Sci. Tech. 45 (1986) 101-113.

[4] F. Morandini, A. Simeoni, P.A. Santoni, J.H. Balbi, Comb. Sci. Tech. 177 (2005) 1381-1418.

[5] B. Porterie, D. Morvan, J.C. Loraud, M. Larini, Phys. Fluids 12 (2000) 1762-1781.

[6] A.M. Grishin, Mathematical Modeling of ofrest fires and new methods of fighting them, Publishing House of the Tomsk State University, Tomsk, Russia, 1997, p. 390.

[7] N. Peters, R.J. Kee, Combust. and Flame 68 (1987) 17-29.

[8] M.J. Safi, I.M. Mishra, B. Prasad, Thermochim. Acta 412 (2004) 155-162.

[9] E.H. Chui, G.D. Raithby, Num. Heat Trans. Part B 23 (1993) 269-288.

[10] H.A. McGhee, Molecular Engineering. McGraw-Hill, New York, 1991, p. 480.

[11] S.V. Patankar, Numerical Heat Transfer and Fluid Flow. Hemisphere Publishing Corporation, Washington, D.C, 1980, p. 197.

[12] B. R. Hutchinson, G.D. Raithby Num. Heat Trans. 9 (1986) 511-537.

[13] F.L. Dryer, I. Glassman, Proc. Combust. Inst. 14 (1973) 987-1003.

[14] D. Morvan, J. L. Dupuy, Combust. and Flame 138 (2004) 199-210.

7 List of figure captions

Fig. 1. a) Time evolution of the mass loss for the three fuels, b) Mass flow rate after 60 s for the three fuels.

Fig. 2. Time evolution of the flame radius for the three species after 60 s.

Fig. 3. Temperature for *Erica arborea* a) along the flame axis, b) horizontally at 1 cm high.

Fig. 4. Comparison between experimental and numerical temperatures obtained with the two gas mixtures along the flame axis for Pinus laricio at 60 s.

Fig. 5. Experimental and predicted temperatures obtained with the different mechanisms along the flame axis for Pinus laricio at 60 s.

Fig. 6. Comparison between experimental and numerical temperatures along the flame axis for a) *Pinus halepensis,* b) *Pinus laricio,* c) *Erica arborea* at 80 s.

Fig. 7. Comparison between experimental and numerical temperatures at 1 cm high for a) *Pinus halepensis,* b) *Pinus laricio,* c) *Erica arborea* at 80 s.

Table 1. Mass fractions of the main pyrolysis gases released by the degradation of the three samples.

Gas	*Pinus halepensis*	*Pinus laricio*	*Erica arborea*
CO_2	0.663	0.616	0.718
H_2O	0.070	0.074	0.047
CO	0.150	0.140	0.141
CH_4	0.032	0.040	0.026
C_2H_x	0.018	0.024	0.011
C_3H_x	0.012	0.016	0.007
C_4H_x	0.055	0.090	0.052
H_2	0.000	0.001	0.000

Table 2. Initial inputs used for the numerical simulations of the flames of the forest fuels.

Fuel	*Pinus halepensis*	*Pinus laricio*	*Erica arborea*
Mechanism		M3	
CO	0.150	0.140	0.141
CH_4	0.032	0.040	0.026
H_2O	0.070	0.074	0.047
CO_2	0.748	0.616	0.718
Burner Radius (cm)	1.48	1.25	1.01
Mass flow rate ($mg.s^{-1}$)	3.27	3.00	3.15

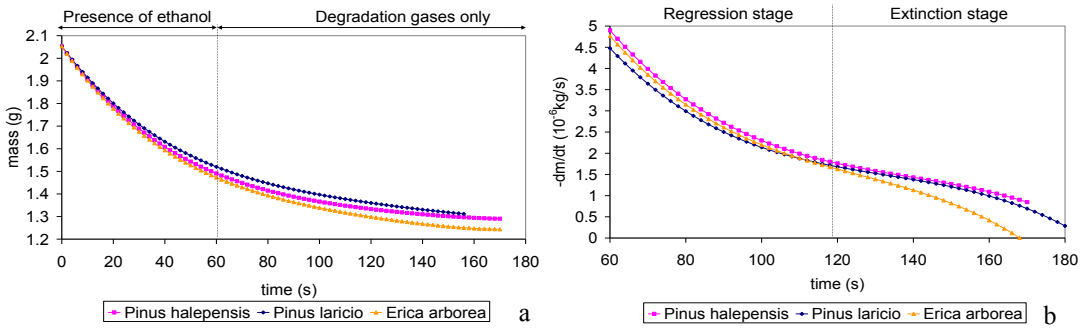

Fig. 1. a) Time evolution of the mass loss for the three fuels, b) Mass flow rate after 60 s for the three fuels.

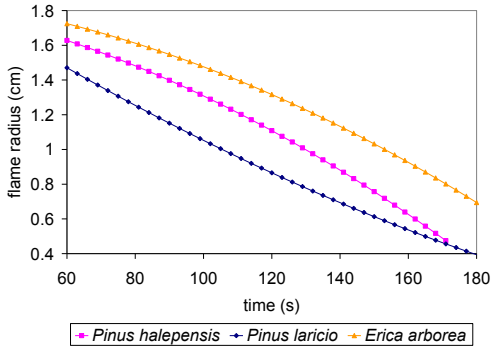

Fig. 2. Time evolution of the flame radius for the three species after 60 s.

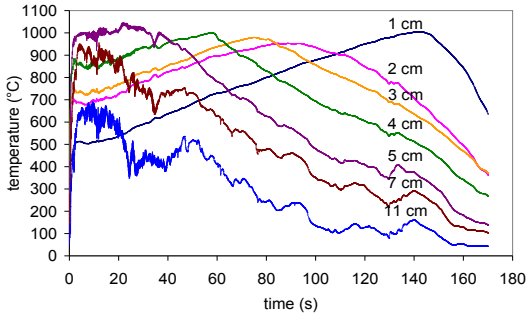

Fig. 3. Temperature for *Erica arborea* along the flame axis.

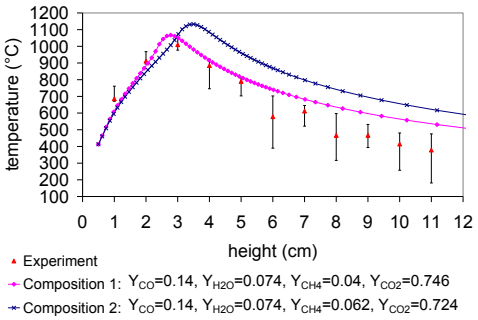

Fig. 4. Comparison between experimental and numerical temperatures obtained with the two gas mixtures along the flame axis for *Pinus laricio* at 60 s.

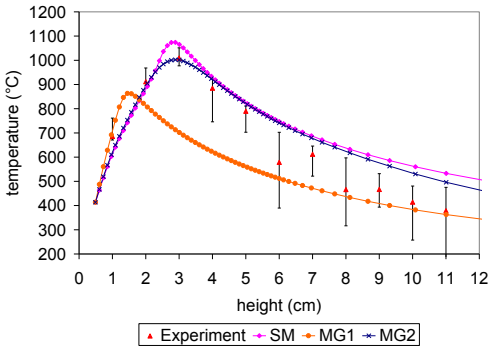

Fig. 5. Experimental and predicted temperatures obtained with the different mechanisms along the flame axis for *Pinus laricio* at 60 s.

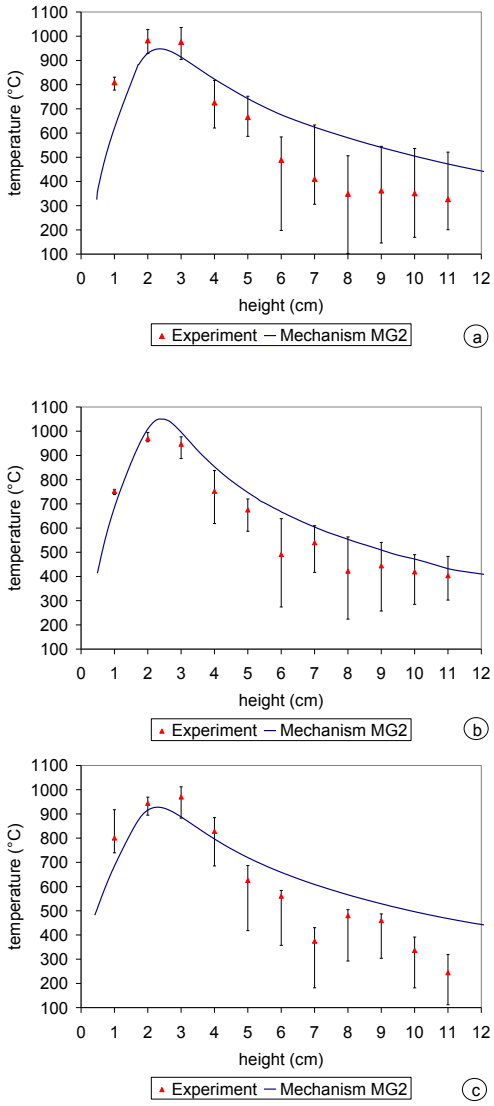

Fig. 6. Comparison between experimental and numerical temperatures along the flame axis for a) *Pinus halepensis,* b) *Pinus laricio,* c) *Erica arborea* at 80 s.

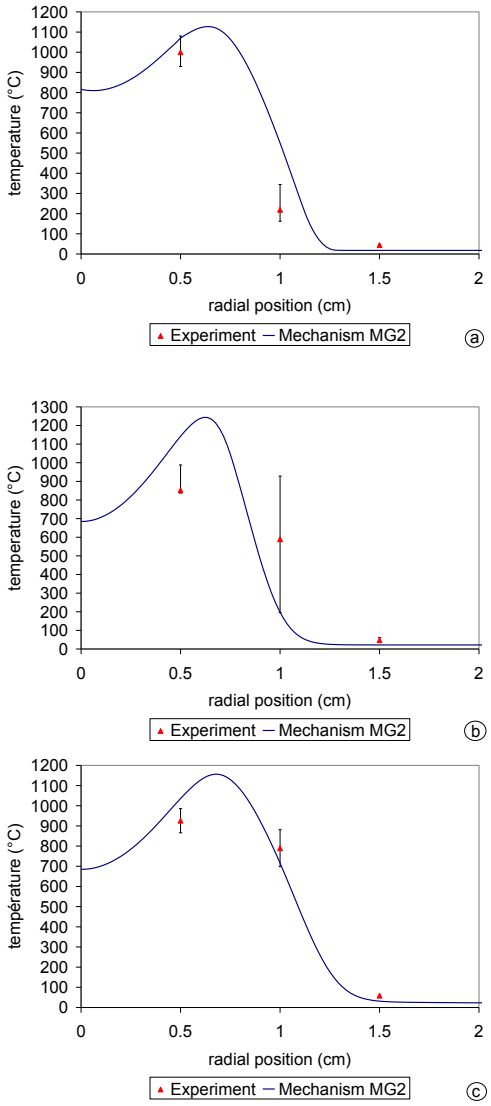

Fig. 7. Comparison between experimental and numerical temperatures at 1 cm high for a) *Pinus halepensis,* b) *Pinus laricio,* c) *Erica arborea* at 80 s.